Effective contact model for geometry-independent conductance calculations in graphene

D. A. Bahamon, A. H. Castro Neto, and Vitor M. Pereira
Graphene Research Centre and Department of Physics, National University of Singapore, 2 Science Drive 3, 117542 Singapore
(Received 21 October 2013; published 27 December 2013)

A geometry-independent effective model for the contact self-energies is proposed to calculate the quantum conductance of patterned graphene devices using Green's functions. A Corbino disk, being the simplest device where the contacts cannot be modeled as semi-infinite ribbons, is chosen to illustrate this approach. This system's symmetry allows an analytical solution against which numerical calculations on the lattice can be benchmarked. The effective model perfectly describes the conductance of Corbino disks at low-to-moderate energies, and is robust against the size of the annular device region, the number of atoms on the edge, external magnetic fields, or electronic disorder. The contact model considered here affords an expedient, flexible, and geometry-agnostic approach that easily allows the consideration of device dimensions encompassing several million atoms, and realistic radial dimensions of a few hundreds of nanometers.

DOI: 10.1103/PhysRevB.88.235433 PACS number(s): 73.23.−b, 73.63.−b, 81.05.ue

To understand the transport properties and predict the performance of nanodevices it is necessary to fabricate appropriate contacts.[1] Their reduced size and different geometries have led to successive reevaluations of existing techniques and processes developed to contact bulk materials.[2] Irrespective of the particularities of the material of the contact, the device, or their geometry, one mainly seeks (i) an Ohmic contact to detect any nonlinearity in the device, and (ii) low resistance to ensure that the properties measured are those of the device and not those of the contact-device interface.[1] One of the preferred tools to theoretically simulate and extract transport characteristics of low-dimensional devices resorts to the calculation of nonequilibrium Green's functions (GFs) for the system composed of the device and the contacts.[3–8] Its appeal stems from its generality and versatility to include in the calculation arbitrary geometries of the device, all kinds of external potentials or interactions, electronic disorder, etc. Within this framework, in the case of a two-dimensional (2D) system the contacts are generally modeled as semi-infinite ballistic ribbons, which automatically satisfy the requirement that electrons enter and exit the device easily, without returning to it.[6,7,9,10]

Graphene, because of its exceptional mechanical and electronic properties,[11] has been called upon to replace existing materials in traditional devices such as high-frequency and logic transistors,[12] photodetectors,[13] optical modulators,[14] etc. Its intrinsic two-dimensionality and mechanical robustness is also expected to foster a revolution in flexible electronics,[15] bio-applications,[16] and energy generation and storage.[17] In current and potential applications relying on the electronic degrees of freedom, graphene devices must be contacted to a metallic lead. Therefore understanding how the contact itself impacts the performance of the device is of critical importance, both fundamentally and on a more applied level.[18–21]

In quantum transport calculations in the context of graphene there are a variety of commonly used and accepted models for a contact that meet the requirements mentioned above. Common to nearly all these models is the fact that the contact geometry eventually converges to a ballistic semi-infinite ribbon at some distance from the contact/graphene interface. When the electron dynamics is described within the effective Dirac equation approach (i.e., a continuum Hamiltonian, rather than a lattice one) contacts are frequently modeled as infinitely doped graphene.[22] In the tight-binding model, on the other hand, contacts can be either modeled as ideal graphene (hexagonal lattice),[23] as an ideal metal (square lattice),[24–26] or using effective models in which the effects of the contacts, are reduced to a constant self-energy value.[24,27,28] Whether the contact/graphene interface is narrow or extended, and whether graphene is side or edge contacted, is another detail that can lead to different conductance features.[29] Given that many of the future and most unexpected applications of graphene in electronics will likely rely on patterning graphene or transferring it to arbitrarily shaped substrates,[30] these tried and tested models of contacts might not always be applicable or correct.

This paper describes an approach to circumvent the difficulties posed by these conventional contact models in more generic device layouts. It proposes a strategy towards a generic geometry-independent model for the contacts, that are then coupled to the usual geometry-dependent tight-binding Hamiltonian for the device. The key assumption is that the contacts inject a large number of modes close to the Dirac point so that the transport through the devices does not depend critically on the specific details (the precise mode structure) of the contacts, and their effect can be very well captured by an effective self-energy term within the GF's framework.[24] This allows an expediient, flexible, and geometry-agnostic approach which easily allows the consideration of device dimensions encompassing more than 5 million atoms, and realistic radial dimensions of a few hundreds of nanometers. The flexibility of the method is illustrated with calculations including two types of disorder, which do not add any significant computational overhead.

Below we describe this effective-contact approach using the conductance calculation in a Corbino geometry as a specific example of its application to graphene devices patterned in a nonconventional way. The Corbino disk is, in a way, the simplest device for which the contact layout is nontrivial, and consists of an annular device region sandwiched between two concentric, highly doped, graphene contacts (Fig. 1). Despite its importance in the context of understanding the integer quantum Hall effect there are only a few studies of ballistic Corbino disks for either Dirac[31,32] or Schrödinger[33–35]

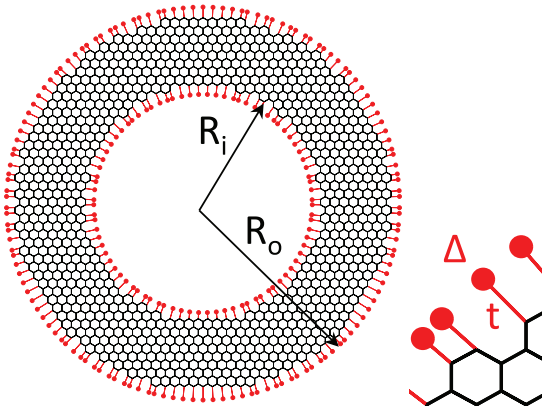

FIG. 1. (Color online) Left panel: lattice representation of a graphene Corbino disk of inner radius R_i and outer radius R_o contacted to an effective contact. Right panel: a closeup of an edge region showing a schematic of graphene atoms bound to the effective contact.

electrons. Moreover, the circular symmetry, despite a complication for the traditional contact models, allows an analytical calculation of the conductance, which we will be using as a benchmark for the GF calculation in the ballistic case. After thus establishing the robustness of the conductance with respect to variations in the number of atoms in the annulus, or at the edges, the effective-contact model is used within the GF framework to probe the effect of disorder and magnetic fields on the conductance of the Corbino disk. The results are in perfect agreement with what is expected from physical grounds, as well as related previous calculations on bulk graphene or graphene nanoribbons.

I. METHOD

A. Conductance: Dirac equation

To understand the basic features of the conductance, and to have a conductance trace against which to benchmark our results for the lattice model, we outline the procedure to extract the conductance using the continuum Dirac description.[31] The single-valley Hamiltonian of graphene can be written as $\hat{H} = \hat{H}_0 + U\sigma_0$, where

$$\hat{H}_0 = -i\hbar v_F \begin{pmatrix} 0 & e^{-i\phi}\{\partial_r - \frac{i}{r}\partial_\phi\} \\ e^{i\phi}\{\partial_r + \frac{i}{r}\partial_\phi\} & 0 \end{pmatrix}. \quad (1)$$

Since $\hat{H}$ commutes with the total angular momentum operator $\hat{J}_z = -i\hbar\partial_\phi + \hbar\sigma_z/2$, the energy eigenstates with energy $E = \tilde{E} - U$ have the form

$$\psi_j(r,\phi) = e^{(j-1/2)\phi}\begin{bmatrix} \chi_{1,j}(r) \\ e^{i\phi}\chi_{2,j}(r) \end{bmatrix} \equiv e^{(j-1/2)\phi}\chi_j(r), \quad (2)$$

where $j = \pm 1/2, \pm 3/2, \ldots$ is the eigenvalue of $\hbar^{-1}\hat{J}_z$. Without loss of generality it is assumed that (i) there is an infinite electron doping $E = \tilde{E} - U_\infty > 0$ in the contacts, and (ii) electrons incident from the inner contact ($r \leqslant R_i$) are scattered in the Corbino disk ($R_i \leqslant r \leqslant R_o$) and finally collected in the outer contact ($R_o \leqslant r$). Under these assumptions, the radial component of the wave function in each region is written as

$$\chi_j^i = \begin{bmatrix} H^1_{j-1/2}(K_\infty r) \\ iH^1_{j+1/2}(K_\infty r)e^{i\phi} \end{bmatrix} + r_j \begin{bmatrix} H^2_{j-1/2}(K_\infty r) \\ iH^2_{j+1/2}(K_\infty r)e^{i\phi} \end{bmatrix}, \quad (3)$$

$$\chi_j^c = a_j \begin{bmatrix} H^1_{j-1/2}(kr) \\ iH^1_{j+1/2}(kr)e^{i\phi} \end{bmatrix} + b_j \begin{bmatrix} H^2_{j-1/2}(kr) \\ iH^2_{j+1/2}(kr)e^{i\phi} \end{bmatrix}, \quad (4)$$

$$\chi_j^o = t_j \begin{bmatrix} H^1_{j-1/2}(K_\infty r) \\ iH^1_{j+1/2}(K_\infty r)e^{i\phi} \end{bmatrix}, \quad (5)$$

where $H_n^{1(2)}(kr)$ is the Hankel function of the first (second) kind and $k = E/(\hbar v_F)$; for the highly doped contacts $K_\infty = (\tilde{E} - U_\infty)/(\hbar v_F)$ with $U_\infty \to -\infty$. The transmission t_j and reflection r_j amplitudes for each channel are obtained by the matching conditions $\psi_j^i(R_i) = \psi_j^c(R_i)$ and $\psi_j^c(R_o) = \psi_j^o(R_o)$. Introducing the transmission probability per angular momentum channel, $T_j = t_j t_j^*$, the conductance of a graphene Corbino disk (including the valley degeneracy) reads[31,33]

$$G = \frac{4e^2}{h}\sum_j T_j. \quad (6)$$

This expression allows a direct computation of the conductance as a function of the Fermi energy. When the conductance obtained from Eq. (6) is compared with the GF calculation on the lattice the dimensionless radial coordinate kr is related to the tight-binding hopping parameter t and the carbon-carbon distance $a = 0.142$ nm via $kr = \frac{2}{3}(\frac{E}{t})\frac{r}{a}$.

B. Conductance: Lattice Green's functions

The starting point of any conductance calculation for noninteracting electrons using GFs is Caroli's formula:[4–6]

$$G = \frac{2e^2}{h}\mathrm{Tr}[\Gamma_q G^r \Gamma_p G^a]. \quad (7)$$

Here $G^r = [G^a]^\dagger = [E + i\eta - H - \Sigma_p - \Sigma_q]^{-1}$ is the retarded GF, $\Gamma_q = i[\Sigma_q - \Sigma_q^\dagger]$ reflects the coupling between the contacts and the device, and Σ_q is the self-energy of contact q. Equation (7) has been extensively used in ribbon geometries where one contact is to the left and the other to the right of the device region.[6,23] The device region can have different shapes or can be connected with more than two contacts; however, each contact has been almost invariably modeled as a semi-infinite ribbon.[36–38] In a Corbino disk an annulus-shaped device region is located between two concentric metallic contacts. Equation (7) holds for any contact layout, and device pattern, provided that the contacts and device are assumed to have been disconnected in the far past.[4,8] The total Hamiltonian is then expressed in terms of three contributions,

$$\hat{H} = \hat{H}_q + \hat{H}_d + \hat{H}_T,$$

which are the contact Hamiltonian

$$\hat{H}_q = \sum_{k\alpha}\epsilon_{k\alpha}c^\dagger_{k\alpha}c_{k\alpha},$$

the device or central Hamiltonian

$$\hat{H}_d = \sum_n \epsilon_n d_n^\dagger d_n + U(d_n^\dagger, d_n),$$

where $U(d_n^\dagger, d_n)$ is a one-body potential, and the contact-device tunneling Hamiltonian

$$\hat{H}_T = \sum_{k,\alpha,n} [V_{k\alpha,n} c_{k\alpha}^\dagger d_n + \text{H.c.}].$$

Combining this with the expression for the current from contact q, $J_q = -e\langle \dot{N}_q \rangle = -ie/\hbar[\hat{H}, \hat{N}_q]$, one obtains Eq. (7).[4,8] The geometry of the device region is easily included in the $\hat{H}_d$ term and the geometry of the contacts is encoded in the self-energy term. In a tight-binding representation the latter is simply expressed as

$$\Sigma_q = V_{dq} g_q V_{qd},$$

where $V_{dq(qd)}$ are the hopping matrices between the device and the contact, and g_q is the GF of the isolated contact. In a generic situation where the geometry of the contacts is not amenable to modeling as a semi-infinite ribbon, or any other simple geometry allowing an analytical form, obtaining g_q and its tight-binding representation would, in principle, be the most challenging step. Irrespective of the geometry or model used for the contacts the self-energy is a complex function, $\Sigma_q = \Lambda - i\Delta$,[6] the real part describing the shift of the energy levels in the device, and the imaginary part the broadening of those same levels. Assuming that the contact has an approximately constant density of states (DOS) around the Fermi energy of the device, and that the contact only affects atoms at the edge, the self-energy can be simplified to a diagonal form,

$$\Sigma_q = -i\Delta = -i\pi\rho_c |t_{dq}|^2, \tag{8}$$

where ρ_c is the contact DOS per atom at the Fermi level,[6,39] and t_{dq} is the coupling between the contact and the device.

Transport calculations in graphene are expected to be insensitive to the contact model used, provided that the contacts inject a large number of modes close to the Dirac point.[24] One way to guarantee that is to model $\rho_c = \rho_{\text{graphene}}(E = t) = 2t/(\sqrt{3}\pi t^2) = 2/(\sqrt{3}\pi t)$, with t being the graphene tight-binding hopping amplitude. In the tight-binding problem, the highest DOS occurs precisely at $E = t$, where the spectrum exhibits a van Hove singularity. Hence, in order to mimic a highly doped graphene contact, it is natural to set its Fermi level at the van Hove singularity. Under these assumptions the self-energy term can then be set to

$$\Sigma_q = -i(2/\sqrt{3})t \approx -it, \tag{9}$$

where, in addition to replacing ρ_c as described above in Eq. (8), we assumed a smooth junction between the contacts and the device: $t_{dq} = t$. For the definite case of the Corbino disk that we shall be concentrating on, the Hamiltonian of the device (annulus) consists of a nearest-neighbor uniform tight-binding approximation. The system is finite, its extent at the microscopic level being determined by the condition $R_i \leqslant r \leqslant R_o$ for the distance, r, of an atom to the origin (see Fig. 1). The local, on-site energy of the atoms with only two neighbors (located at the inner and outer edges) is modified by the self-energy term $-it$, and the device conductance is calculated using Eq. (7).

We note that, as an alternative to a conductance calculation in the actual honeycomb lattice, the circular symmetry suggests a polar grid discretization of the wave equation,[40] which could in principle afford an opportunity to simulate ideal metallic contacts. As an illustration, the contact GF of an effective annular metallic contact is presented in Appendix. Unfortunately, the conductance obtained by this scheme is highly sensitive to the contact and coupling parameters because a commensurate lattice discretization in the contacts is not possible due to the irregularity of the edges in the graphene annulus (see Fig. 1). This fact restricts the proper injection of contact modes across the junction and, as underlined in the introductory section, the calculated conductance becomes dominated by the properties of this junction, rather than by the intrinsic behavior of the target annulus region.

II. DIRAC EQUATION VS GREEN'S FUNCTIONS

To easily compare the values of conductance in Corbino disks of different aspect ratio R_i/R_o calculated via the Dirac equation Eq. (6) and the lattice GFs Eq. (7), we normalized the conductance by R_i.[31] The meaning of this normalization procedure will be addressed in the next section. In Fig. 2(a) the normalized conductance is shown as a function of the Fermi

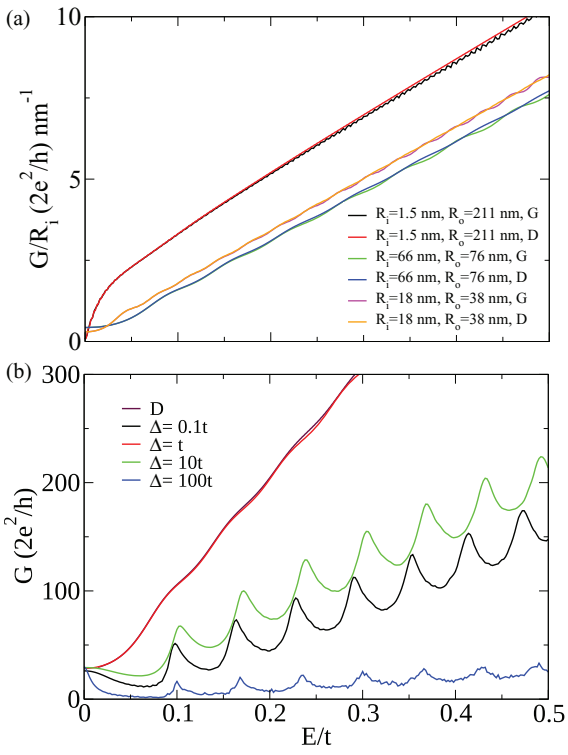

FIG. 2. (Color online) (a) Energy dependence of the conductance normalized by R_i for different values of R_i and R_o, calculated using Eq. (6) (labeled "D") and the lattice Green's function approach (labeled "G"). (b) Conductance of a Corbino Disk with $R_i = 66$ nm and $R_o = 76$ nm using the Green's function approach with the effective self-energy term $\Sigma_q = -i\Delta$, for different values of Δ. The line labeled by "D" was calculated using Eq. (6)

energy in the annulus region for $R_i/R_o = 0.007, 0.86, 0.47$. This range of geometric parameters was chosen to analyze the effect of the disk size (number of atoms) on the conductance, and also to allow us to probe the effect of varying the number of edge atoms (which, as advanced above, have their on-site energy modified by the self-energy term). These three aspect ratios are achieved in practice with three devices with the following characteristics, in order: (i) a wide annulus defined by $R_i = 1.5$ nm and $R_o = 211$ nm, with a very large number of carbon atoms ($N = 5\,337\,206$), and a large unbalance between the number of atoms on the inner ($n_i = 42$) and outer edges ($n_o = 5940$); (ii) a narrow annulus with $R_i = 66$ nm and $R_o = 76$ nm made out of $N = 170\,046$ atoms, and having a similar number of edge atoms ($n_i = 1860$, $n_o = 2142$); (iii) an intermediate case with $R_i = 18$ nm and $R_o = 38$ nm having $N = 134\,631$ atoms, and with a n_i/n_o ratio of about half ($n_i = 510$, $n_o = 1071$). From Fig. 2(a) it is evident that the conductance calculated using GFs (G_G) agrees with the conductance obtained via the Dirac equation (G_D), irrespective of the geometric parameters. For all geometries both methods lead to conductance traces that are hardly distinguishable in the plot. Indeed, for the whole energy range shown in this figure, the relative difference between the two calculation methods is smaller than 2%, confirming that taking $\Delta = t$ produces a smooth effective coupling between the highly doped graphene contacts and the graphene annulus.

In simplified models the contact can be treated as a quantum wire in the wide-band limit ($t \to \infty$), which leads to an imaginary constant self-energy term ($-i\Delta$). The conductance calculated in that framework oscillates when the number of atoms in the device (N), the number of atoms on the edges ($n_{i(o)}$), or the value of Δ are changed.[27,41] Figure 2(a) shows oscillations in $G_{D(G)}/R_i$, which are more pronounced in the GF method due to the roughness of the edges, the scattering at the edges is also responsible for the slightly lower value of G_G. The period of the oscillations is related to the annulus' width $W = R_o - R_i$,[31] since it is also observed in G_D and does not depends on the values of N, n_i, or n_o. The conductance of Corbino Disks calculated by the GF method behaves similarly to the simplified wide-band model under changes in Δ,[27,41] as can be seen in Fig. 2(b). Increasing Δ improves transmission until reaching the optimum—compared with the line labeled "D", calculated using Eq. (6)—conductance line shape for $\Delta = t$. Larger Δ values reduce the conductance again until the peaks corresponding to different eigenstates can not be distinguished.[6]

III. BALLISTIC CONDUCTANCE OF A CORBINO DISK

A. Pristine graphene lattice

Having shown that the GF method with an effective self-energy term ($\Sigma_q = -it$) reproduces the ballistic conductance of graphene Corbino disks, we now scrutinize its features in more detail. Setting first $R_i = 1.5$ nm and increasing R_o, Corbino disks of different width are defined. Their conductance characteristic is presented in Fig. 3(a). One observes that, firstly, the conductance at the Dirac point (inset) is higher for narrow disks due to the evanescent states, and when the width increases their effect is reduced and the conductance

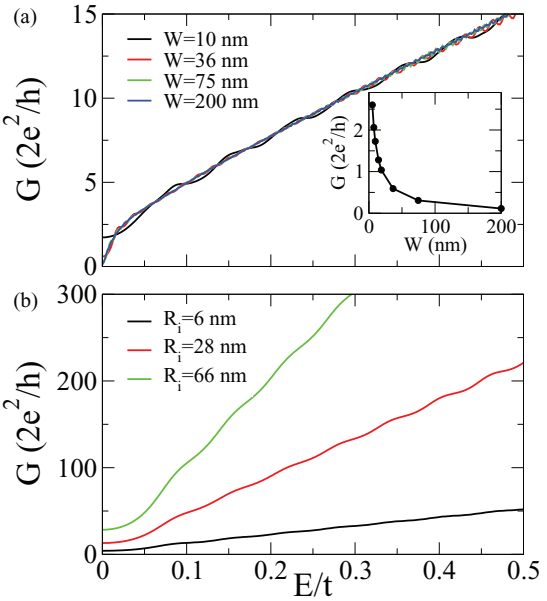

FIG. 3. (Color online) (a) Conductance of a Corbino disk of fixed $R_i = 1.5$ nm and varying width $W = R_o - R_i$. The inset shows the conductance at the Dirac point as function of the width. (b) Conductance of a Corbino disk of fixed width $W = 10$ nm and different values of R_i and R_o.

decreases as $\propto 1/W$,[31] reaching $G = 0.1(2e^2/h)$ for $W = 200$ nm. For higher energies conductance plateaus are not defined due to the highly doped contacts. Secondly, faint Fabry-Perot oscillations slightly modulate the curves of $G(E)$ with a periodicity $\Delta E = \pi\hbar v_F/W$. Finally, regardless of the value of the outer radius, the conductance increases linearly with the Fermi energy. The slope obtained from Fig. 3(a) is 23.56 in units of $(2e^2E/ht)$. This value can be extracted from Eq. (6) with a semiclassical argument assuming that the propagating angular momentum channels are transmitted with probability one, and that, for a given energy $E = v_F\hbar k_F$, the maximum angular momentum eigenmode that can propagate is determined by $j_{\max} \sim \hbar k_F R_i$ when $k_F R_i \gg 1$. Under these conditions $G \approx (4e^2/h)2j_{\max} = (4e^2/h)2(2/3a)R_i(E/t)$ which, for $R_i = 1.5$ nm used in Fig. 3, means a slope of 28.17. The discrepancy between this estimate and the numerical slope simply reflects the fact that the transmission probability is not 1 for all the angular momentum channels, as can be expected from the fact that the effective radial potential depends on the angular momentum.[33] From the discussion above one should expect higher values of conductance for higher inner radii. This is confirmed in Fig. 3(b) where the conductance is calculated for fixed $W = 10$ nm and varying R_i. The effect of a higher R_i is not only a larger slope in the $G(E)$ traces at high energies, but also a higher conductance at the Dirac point by virtue of the fact that larger inner radii support more total angular momentum channels, and hence more modes can be injected into the device. Near the Dirac point the conductance is linear in R_i and energy independent. This occurs in an energy range $\Delta E \sim 3a/4R_i$, and this energy scale can be obtained within a semiclassical approximation recalling that near the Dirac point only one value of total angular momentum is allowed:

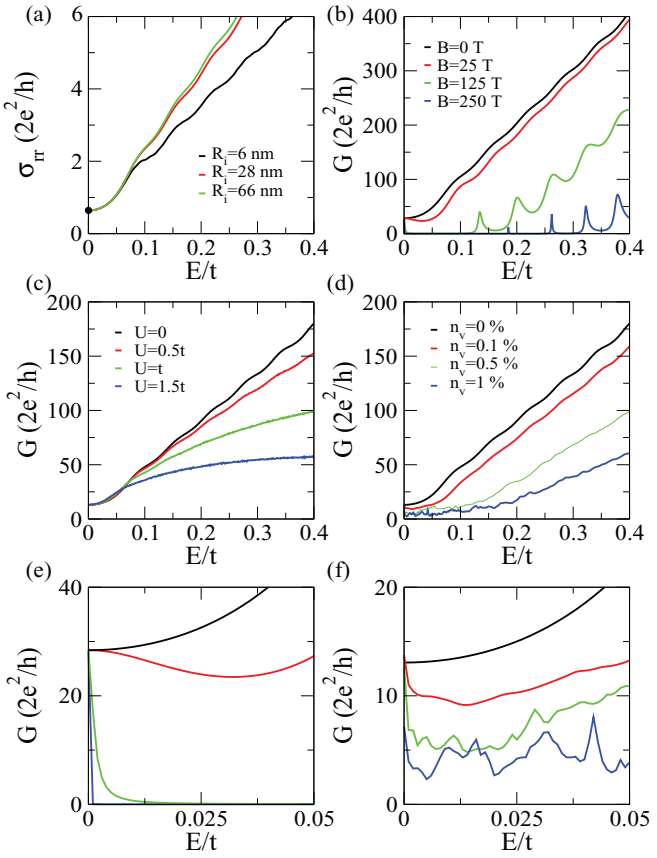

FIG. 4. (Color online) (a) Radial conductivity of a Corbino disk with fixed width $W = 10$ nm and different values of R_i and R_o. The black dot in the vertical axis marks the value of the universal minimum of conductivity, $\sigma_0 = 4e^2/\pi h \approx 0.6(2e^2/h)$. (b) Conductance of a Corbino disk having $R_i = 66$ nm and $R_o = 76$ nm for different values of an external, perpendicular, and homogeneous magnetic field, B. The panels in the second row show the conductance of a Corbino disk having $R_i = 28$ nm and $R_o = 38$ nm with on-site disorder (c), and a finite density of vacancies (d). In (e) and (f) we present a closeup of the low-energy region for the curves in (b) and (d), respectively.

$kR_i = 1/2$. The radial conductivity defined by[31,42]

$$\sigma_{rr}(E) = G(E)\left[\frac{1}{2\pi}\ln\frac{R_o}{R_i}\right] \tag{10}$$

can be seen to collapse on a single curve at the lowest energies, and then eventually on a single point at $E = 0$, irrespective of the value of R_i for narrow annuli ($R_i/R_o \approx 1$). This universal value corresponds to the well known universal minimum of conductivity $\sigma_0 = 4e^2/\pi h \approx 0.6(2e^2/h)$, whereas for high energies the trace of σ_{rr} fans out with a slope that is geometry dependent.

In Fig. 4(b) one can see the effect of a constant magnetic field B on the conductance calculated using GFs for a Corbino disk of $R_i = 66$ nm and $W = 10$ nm. The conductance line-shape can be straightforwardly understood by direct comparison of the electron's cyclotron radius $r_c = \ell_B^2 k_F$ ($\ell_B = \sqrt{\hbar/eB}$ is the magnetic length) with the width (W) of the disk.[32,33] As long as $r_c < W/2$ the electrons entering from the inner contact cannot reach the outer one, which leaves only the possibility of transmission via Landau level (LL) assisted resonant tunneling.[43] This explains the resonant structure of $G(E)$ at precisely the energies $E_n = (\hbar v_f/\ell_B)\sqrt{2n}$, as observed in this figure when $B = 250$ T or $B = 125$ T. For example, when $B = 250$ T the maximum energy shown in the plot ($E \approx 0.4t$) corresponds to $r_c = W/2$, which explains the sharp resonant peaks at $E = 0, 0.18t, 0.26t, 0.32t, E_4 = 0.37t$. But if $B = 125$ T, resonant peaks are observed only at $E = 0, 0.13t$ because at $E \approx 0.2t$ the cyclotron radius is already $r_c = W/2$, and hence the third peak at $E = 0.18t$ is not perfectly defined. When $r_c > W/2$ the injected electrons reach the outer contact and the conductance grows linearly in energy. This is seen in all cases beyond the particular energy above which that condition holds. Notably, the conductance at $E = 0$ remains pinned to its zero-field value, irrespective of the presence or magnitude of the magnetic field.[43] This is shown explicitly in Fig. 4(e) where we magnify the low-energy range of the curves in Fig. 4(b): the effect of the magnetic field is to sharpen or narrow the conductance peak at $E = 0$, without changing its amplitude.

B. Disordered graphene

The results discussed up to this point have not merely tested the robustness and accuracy of the effective self-energy term, but all the results have been related and explained on physical grounds. We have seen that the GF method perfectly describes the conductance and conductivity of Corbino disks of different aspect ratios R_i/R_o, with and without magnetic field, and for a wide range of Fermi energies. The next step is to take advantage of the versatility of the GF technique to include disorder. Despite the vast amount of studies and attention dedicated to effects of disorder in graphene bulk and nanoscale systems,[44,45] the Corbino geometry remains unexplored. Since it is well known that the results are affected by the geometry of the sample and the model of disorder used, such studies are pertinent and relevant, and we proceed now to offer a perspective over some of the peculiarities of this problem. The disordered case has been approached for a representative system starting with a graphene Corbino disk of $R_i = 28$ nm and $R_o = 38$ nm, to which Anderson on-site disorder or a finite density of lattice vacancies was added. The extracted conductance is then averaged over 30 disorder realizations. The results for Anderson disorder are reported in Fig. 4(c), where the on-site energy is uniformly distributed within $[-U/2, U/2]$, and we have considered disorder strengths of $U = 0.5t, t, 1.5t$. At low energies it is clear that the conductance is only modestly affected by the on-site disorder. This is due to the fact that for $E/t \lesssim 3a/4R_i$ the conductance is dominated by tunneling across the entire system via evanescent states, and hence $\sigma_{rr}(E \sim 0) = \sigma_0$. The origin of this energy scale can be seen easily with the same semiclassical argument used earlier, now applied to the minimum energy above which an angular momentum eigenmode is able to propagate through the system: using again the fact that $E = v_F \hbar k_F$, that the angular momentum is quantized in half-integer units with $|j| = 1/2, 3/2, \ldots$, and that the semiclassical angular momentum corresponds to $j \sim \hbar k_F R_i$, then the energy threshold for mode propagation is expected to be $E_{\min} \sim j_{\min} v_F/R_i$; replacing $j_{\min} = 1/2$ leads to $E_{\min}/t = 3a/(4R_i)$. At precisely zero energy a

conformal mapping can transform a nanoribbon with aspect ratio $W/L \gg 1$ into a Corbino disk with $R_i/R_o \approx 1$.[31,37] The aspect ratio of the disk studied in Fig. 4(c) is 0.86, which means that the radial conductance σ_{rr} at $E = 0$ should coincide with the conductance of a nanoribbon in the regime $W \gg L$, which is the so-called pseudodiffusive regime.[31,44,45] Our data shows that this value is indeed obtained and, since $G(E = 0)$ is insensitive to Anderson disorder, the corresponding conductivity can be read directly from Fig. 4(a). Away from the Dirac point the conformal mapping technique ceases to be valid. In this region the conductance decreases as the disorder strength increases, as one expects in general.

In the presence of vacancies or divacancies the conductance of Graphene nanoribbons exhibits dips, asymmetric Fano resonances, or Breit-Wigner peaks.[46] This arises due to the fact that a vacancy creates a localized zero-energy state.[47] The interest in the effect of these zero-energy states and its effect on the electronic transport at the Dirac point has been recently boosted by some experiments[48] and theoretical calculations.[49,50] Within the tight-binding Hamiltonian that we have been considering, a vacancy is easily modeled by setting the hopping parameter between neighboring atoms to zero, or by setting the on-site energy of the vacancy to a value much larger than the energy bandwidth. When a single vacancy is included in the Corbino disk there is no effect on the overall conductance, essentially as a result of the highly doped contacts and the radial current distribution. But a finite density of vacancies, n_v, equally probable on both sublattices,[51] considerably impacts the energy dependence of the conductance, as shown in Fig. 4(d). On the one hand, the conductance is peaked at the Dirac point with a maximum value that is lower than the conductance of the pristine disk and decreases for $n_v > 0.5\%$, while for $n_v \leqslant 0.1\%$ the peak is 5% higher than the pristine conductance, as highlighted in Fig. 4(f). This is reminiscent of the formation of the supermetallic regime discussed in Ref. 50. On the other hand, the conductance exhibits a flat energy behavior up to a much larger energy threshold in comparison with the behavior in the presence of Anderson disorder, and only then starts growing linearly.

IV. SUMMARY

We established that an effective and simplified model for the contact self-energies can be used with high accuracy and robustness in the computation of the quantum conductance from lattice Green's functions of nanostructured graphene devices with arbitrary contact geometry. As a particular example of application, the conductance of graphene Corbino disks was studied in detail using this method, the Corbino disk being chosen strategically for being a geometry with nontrivial contact configuration for GF methods, while at the same time allowing an analytical solution in the Dirac approximation. This permitted the direct comparison and control of the conductance emerging from the GF results using the proposed contact model with the conductance that follows from the exact solutions in the Dirac approximation. Since many envisaged graphene devices and applications entail systems patterned at the nanoscale in various configurations that are not always reducible to planar or linear contact geometries, an effective and geometry-independent contact model such as the one proposed here is certainly a valuable tool for theoretically studying the transport characteristics of such structures. Our proposal simplifies the description of the contact, but is seen as reliable and, more importantly, fulfills the requirements of an ideal contact model, in that it does not introduce any spurious features.[1]

As far as the details of the conductance of the graphene Corbino disk are concerned, the main results discussed here can be summarized first by underlining that the conductance calculated for different aspect ratios R_i/R_o, with and without magnetic field, shows that one key role of the inner contact radius (R_i) is to define the maximum number of allowed total angular momentum channels and, therefore, the slope of $G(E)$ at high energies. The outer radius (R_o) is important insofar as it defines the width of the annulus, affecting the value of conductance near the Dirac point due to tunneling by evanescent states. Finally, we could appreciate how sensitive the conductance trace is to the type of electronic disorder: whereas on-site Anderson disorder is characterized by the "universal" minimum of conductivity (σ_0) at $E = 0$ irrespective of the value of the inner radius, strong disorder induced by vacancies, on the other hand, can lead to conductance values that exceed the pristine situation near $E = 0$, but quickly vanish away from the Dirac point.

ACKNOWLEDGMENTS

We are extremely grateful to Miguel D. Costa for his instrumental collaboration in optimizing portions of the numerical computations, and porting some routines and operations to a numerically sparse implementation. This work was supported by the NRF-CRP grant "Novel 2D materials with tailored properties: beyond graphene" (R-144-000-295-281).

APPENDIX: SCHRÖDINGER CORBINO DISK

To calculate the conductance of a Corbino disk with Schrödinger electrons using GFs it is necessary to discretize the Schrödinger equation on a polar grid. Before discretizing, in order to ensure the Hermiticity of the Hamiltonian, the transformation $\Psi(r,\phi) = \psi(r,\phi)/\sqrt{r}$ is done and the Schrödinger equation is rewritten as

$$-\frac{\hbar^2}{2m_e}\left[\frac{\partial^2}{\partial r^2} + \frac{1}{4r^2} + \frac{\partial^2}{\partial \phi^2}\right]\psi + V(r,\phi)\psi = E\psi. \quad \text{(A1)}$$

On the grid the wave function $\psi(r,\phi)$ is expressed as $\psi_{m,j}$ where the indexes (m,j) represent the radial, $r = m\Delta_r$, and polar, $\phi = j\Delta_\phi$, sites, with Δ_r and Δ_ϕ the radial and angular grid spacing, respectively. Writing Eq. (A1) in a finite difference approximation leads to

$$t_r\psi_{m+1,j} + t_r\psi_{m-1,j} - \left[2t_r + 2t_\phi^m + U_m + V_{m,j}\right]\psi_{m,j} + t_\phi^m\psi_{m,j+1} + t_\phi^m\psi_{m,j-1} = E\psi_{m,j}, \quad \text{(A2)}$$

with the radial hopping, the angular hopping, and the radial potential given, respectively, by

$$t_r = -\frac{\hbar^2}{2m_e\Delta_r^2}, \quad t_\phi^m = -\frac{\hbar^2}{2m_e r_m^2\Delta_\phi^2}, \quad U_m = \frac{\hbar^2}{8m_e r_m^2}. \quad \text{(A3)}$$

In the contacts one assumes that the electrons are under the influence of an effective constant potential. This means that one sets $U_m = \frac{\hbar^2}{8m_e R_{i(o)}^2}$ and $t_\phi^m = -\frac{\hbar^2}{2m_e R_{i(o)}^2 \Delta_\phi^2}$ as constants in Eq. (A2). Under these assumptions the GF of the contacts is calculated as

$$g(E; R_{i(o)}, j, j') = \sum_{l=0}^{N_\phi} \left(\frac{e^{il2\pi j/N_\phi}}{\sqrt{N_\phi}} \right) \frac{e^{i\theta_{i(o)}^l}}{t_r} \left(\frac{e^{-il2\pi j'/N_\phi}}{\sqrt{N_\phi}} \right), \quad \text{(A4)}$$

where N_ϕ is the number of cells in the angular grid and

$$\cos\theta_{i(o)}^l = \frac{E + t_r + 2t_\phi^{i(o)} + U_{i(o)}}{2t_r} - \frac{t_\phi^{i(o)}}{t_r} \cos\left(\frac{2\pi l}{N_\phi}\right). \quad \text{(A5)}$$

Figure 5 shows the result of this approach in the calculation of the conductance of a Corbino disk where the target conducting medium is GaAs ($m_e = 0.067 m_o$), with $R_i = 0.1\ \mu$m and $R_o = 0.2\ \mu$m. The main features of the quantum conductance in a *massive* electronic system such as this one were previously described by Kirczenow.[33] We underline that, despite the fact that one can obtain these analytical expressions for the quantum conductance in this case, it immediately becomes unpractical in any realistic scenario. First, even though metallic contacts can be modeled by Eq. (A4) and coupled to a graphene annulus as described above, the conductance trace is highly sensitive to the contact parameters, which is not an ideal situation. Secondly, the radial decomposition offers little advantage for a geometry that is not perfectly cylindrical, which makes the approach of limited use for general contact geometries. Finally, even when the perfect Corbino layout is considered, the quantization shown in Fig. 5 has not been observed experimentally, which necessarily raises the question of how to treat disorder efficiently within such an approach. That is when calculations based on lattice GFs offer a more flexible and expedient (and, at the same time, less biased, or with less approximations) means of extracting the transport quantities. In fact, as far as the computational effort of the lattice GFs is concerned, the inclusion of disorder has very little detrimental impact.

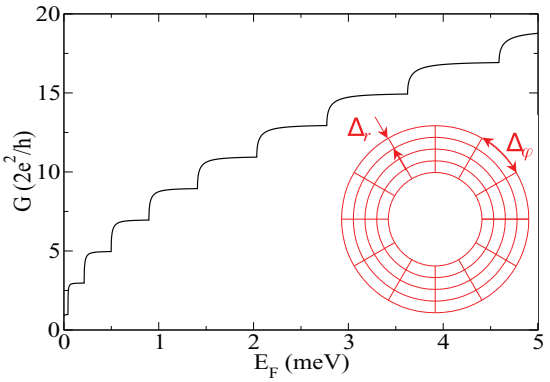

FIG. 5. (Color online) Conductance of a ballistic Corbino disk ($R_i = 0.1\ \mu$m and $R_o = 0.2\ \mu$m) in GaAs as a function of the Fermi energy, E_F. The curve was obtained using the effective contact Green's function Eq. (A4). Inset: schematic of the polar grid used in the finite difference decomposition of the Schrödinger equation.

[1] K. W. Hipps, Science **294**, 536 (2001).
[2] F. Leonard and A. A. Talin, Nat. Nanotechnol. **6**, 773 (2011).
[3] P. A. Lee and D. S. Fisher, Phys. Rev. Lett. **47**, 882 (1981).
[4] Y. Meir and N. S. Wingreen, Phys. Rev. Lett. **68**, 2512 (1992).
[5] C. Caroli, R. Combescot, P. Nozieres, and D. Saint-James, J. Phys. C **4**, 916 (1971).
[6] S. Datta, *Electronic Transport in Mesoscopic Systems* (Cambridge University Press, Cambridge, 1995).
[7] D. K. Ferry and S. M. Goodnick, *Transport in Nanostructures* (Cambridge University Press, Cambridge, 1997).
[8] H. Haug and A.-P. Jauho, in *Quantum Kinetics in Transport and Optics of Semiconductors*, Solid State Sciences Vol. 123 (Springer, Berlin, 2008), pp. 181–212.
[9] T. Ando, Phys. Rev. B **44**, 8017 (1991).
[10] M. P. L. Sancho, J. M. L. Sancho, J. M. L. Sancho, and J. Rubio, J. Phys. F **15**, 851 (1985).
[11] K. S. Novoselov, V. I. Fal'ko, L. Colombo, P. R. Gellert, M. G. Schwab, and K. Kim, Nature (London) **490**, 192 (2012).
[12] F. Schwierz, Nat. Nanotechnol. **5**, 487 (2010).
[13] F. Xia, T. Mueller, Y.-m. Lin, A. Valdes-Garcia, and P. Avouris, Nat. Nanotechnol. **4**, 839 (2009).
[14] F. Wang, Y. Zhang, C. Tian, C. Girit, A. Zettl, M. Crommie, and Y. R. Shen, Science **320**, 206 (2008).
[15] S. Bae, H. Kim, Y. Lee, X. Xu, J.-S. Park, Y. Zheng, J. Balakrishnan, T. Lei, H. Ri Kim, Y. I. Song *et al.*, Nat. Nanotechnol. **5**, 574 (2010).
[16] T. Kuila, S. Bose, P. Khanra, A. K. Mishra, N. H. Kim, and J. H. Lee, Biosens. Bioelectron. **26**, 4637 (2011).
[17] E. Yoo, J. Kim, E. Hosono, H.-s. Zhou, T. Kudo, and I. Honma, Nano Lett. **8**, 2277 (2008).
[18] F. Xia, V. Perebeinos, Y.-m. Lin, Y. Wu, and P. Avouris, Nat. Nanotechnol. **6**, 179 (2011).
[19] S. Barraza-Lopez, M. Vanević, M. Kindermann, and M. Y. Chou, Phys. Rev. Lett. **104**, 076807 (2010).
[20] E. J. H. Lee, K. Balasubramanian, R. T. Weitz, M. Burghard, and K. Kern, Nat. Nanotechnol. **3**, 486 (2008).
[21] B. Huard, N. Stander, J. A. Sulpizio, and D. Goldhaber-Gordon, Phys. Rev. B **78**, 121402 (2008).
[22] J. Tworzydło, B. Trauzettel, M. Titov, A. Rycerz, and C. W. J. Beenakker, Phys. Rev. Lett. **96**, 246802 (2006).
[23] C. Lewenkopf and E. Mucciolo, J. Comput. Electron. **12**, 203 (2013).
[24] H. Schomerus, Phys. Rev. B **76**, 045433 (2007).
[25] J. P. Robinson and H. Schomerus, Phys. Rev. B **76**, 115430 (2007).
[26] Y. M. Blanter and I. Martin, Phys. Rev. B **76**, 155433 (2007).
[27] N. Nemec, D. Tománek, and G. Cuniberti, Phys. Rev. B **77**, 125420 (2008).
[28] V. N. Do and P. Dollfus, J. Phys.: Condens. Matter **22**, 425301 (2010).
[29] S. Krompiewski, Nanotechnology **22**, 445201 (2011).

[30]K. S. Kim, Y. Zhao, H. Jang, S. Y. Lee, J. M. Kim, K. S. Kim, J.-H. Ahn, P. Kim, J.-Y. Choi, and B. H. Hong, Nature (London) **457**, 706 (2009).
[31]A. Rycerz, P. Recher, and M. Wimmer, Phys. Rev. B **80**, 125417 (2009).
[32]A. Rycerz, Phys. Rev. B **81**, 121404 (2010).
[33]G. Kirczenow, J. Phys.: Condens. Matter **6**, L583 (1994).
[34]S. Souma and A. Suzuki, Phys. Rev. B **60**, 15928 (1999).
[35]S. Souma and A. Suzuki, Phys. Rev. B **58**, 4649 (1998).
[36]H. U. Baranger and A. D. Stone, Phys. Rev. B **40**, 8169 (1989).
[37]M. I. Katsnelson and F. Guinea, Phys. Rev. B **78**, 075417 (2008).
[38]Z. Qi, D. A. Bahamon, V. M. Pereira, H. S. Park, D. K. Campbell, and A. H. C. Neto, Nano Lett. **13**, 2692 (2013).
[39]W. Tian, S. Datta, S. Hong, R. Reifenberger, J. I. Henderson, and C. P. Kubiak, J. Chem. Phys. **109**, 2874 (1998).
[40]S. Rotter, J.-Z. Tang, L. Wirtz, J. Trost, and J. Burgdörfer, Phys. Rev. B **62**, 1950 (2000).
[41]V. Mujica, M. Kemp, and M. A. Ratner, J. Chem. Phys. **101**, 6856 (1994).
[42]V. B. Shikin, J. Exp. Theor. Phys. Lett. **66**, 581 (1997).
[43]E. Prada, P. San-Jose, B. Wunsch, and F. Guinea, Phys. Rev. B **75**, 113407 (2007).
[44]N. M. R. Peres, Rev. Mod. Phys. **82**, 2673 (2010).
[45]S. Das Sarma, S. Adam, E. H. Hwang, and E. Rossi, Rev. Mod. Phys. **83**, 407 (2011).
[46]D. A. Bahamon, A. L. C. Pereira, and P. A. Schulz, Phys. Rev. B **82**, 165438 (2010).
[47]V. M. Pereira, F. Guinea, J. M. B. Lopes dos Santos, N. M. R. Peres, and A. H. Castro Neto, Phys. Rev. Lett. **96**, 036801 (2006).
[48]L. A. Ponomarenko, A. K. Geim, A. A. Zhukov, R. Jalil, S. V. Morozov, K. S. Novoselov, I. V. Grigorieva, E. H. Hill, V. V. Cheianov, V. I. Fal'ko *et al.*, Nat. Phys. **7**, 958 (2011).
[49]A. L. C. Pereira and P. A. Schulz, Int. J. Mod. Phys. B **23**, 2618 (2009).
[50]A. Cresti, F. Ortmann, T. Louvet, D. Van Tuan, and S. Roche, Phys. Rev. Lett. **110**, 196601 (2013).
[51]V. M. Pereira, J. M. B. Lopes dos Santos, and A. H. Castro Neto, Phys. Rev. B **77**, 115109 (2008).